

## Observation of Defect-Assisted Magnetic Vortex Core Reversal at Ultralow Critical Velocity

Mahdi Mehrnia,<sup>1</sup> Jeremy Trimble,<sup>1</sup> Olle Heinonen,<sup>2</sup> and Jesse Berezovsky<sup>1,\*</sup>

<sup>1</sup>*Department of Physics, Case Western Reserve University, Cleveland, Ohio 44106, USA*

<sup>2</sup>*Materials Science Division, Argonne National Laboratory, Lemont, Illinois 60439, USA*

 (Received 15 October 2020; revised 11 June 2021; accepted 20 August 2021; published 28 September 2021)

The stability of structures with nontrivial topology is a subject of great interest, both from fundamental and technological perspectives. The topology of a magnetic vortex, for example, results in high stability of the vortex core polarity, which is attractive for applications. This high stability, however, greatly impedes the required deterministic polarity switching, which is typically only achieved with large magnetic fields or strong dynamic driving. Here, we show that the interaction between the vortex core and manufactured nanoscale defects in the magnetic material lowers the required driving strength for core polarity reversal by more than an order of magnitude. We excite vortex dynamics in thin permalloy disks, and map the two-dimensional (2D) vortex core trajectory using 3D time-resolved Kerr microscopy. In pristine samples, we observe normal gyrotropic motion of the vortex core. After laser-induced generation of defects, however, we observe repeated vortex core reversal at much-reduced driving strength. Micromagnetic simulations reveal how local reduction of exchange coupling and saturation magnetization can create vortex core reversal sites for deterministic vortex core switching.

DOI: [10.1103/PhysRevApplied.16.034049](https://doi.org/10.1103/PhysRevApplied.16.034049)

### I. INTRODUCTION

The large energy barrier between the two polarity states of a magnetic vortex core (VC) makes it stable against a polarity switch, such that an out-of-plane static field of about 0.5 T is required to switch a static vortex core [1]. The stability of topologically protected vortices and related magnetic textures such as skyrmions makes them potential candidates for nonvolatile information storage and processing [2–9], and the resulting dramatic reversal processes offer potential as microwave emitters [10,11]. For applications, we require a method to switch the polarity that is fast, efficient, and deterministic. On the other hand, to switch the VC polarity as a topological defect, the creation or annihilation of topological defects in a soft magnetic material only occurs if there is a conservation of the topological charge [12–14]. In the case of dynamic driving, it has been shown that switching can be achieved by reaching a well-defined threshold in the exchange energy density, corresponding to energy necessary for the formation of a vortex-antivortex-vortex structure in order to switch the core polarity at small magnetic fields [15]. By dynamically driving the VC, a wake with polarity opposite to the VC forms and trails behind the VC [16,17]. At sufficiently strong driving, this wake, also called a dip particle, forms a new antivortex-vortex pair in the neighborhood of

the initial VC. The antivortex annihilates the initial vortex core and the result is a new vortex core that has the polarity opposite to the initial vortex core [16,18,19]. In previous works, it has been shown that, by driving the VC to a critical velocity  $v_c \approx 1.66\gamma\sqrt{A}$  ( $\gamma$  is the gyromagnetic ratio and  $A$  is the exchange stiffness), one can produce the vortex-antivortex-vortex and thereby switch the VC [16,18,20–24]. Although many demonstrations of VC reversal depend on exceeding this critical velocity, switching with weaker excitation can be achieved by altering the shape of the structure, or with more complex driving fields. In these cases, vortex core speed may not be the main criterion for core reversal, yet still provides a key figure of merit as a measure of the required magnitude of excitation for reversal. In Ref. [25], the authors demonstrate a vortex core reversal in permalloy elliptical disks at velocities as low as 195 m/s, which is below the predicted value  $v_c = 340$  m/s. In this case, the elliptical shape of the disks help to lower the stability of the VC in motion and results in the formation of the vortex-antivortex-vortex system at velocities lower than the theoretical prediction. Also, in Ref. [26], the authors observed VC reversal at velocities as low as 100 m/s in thin permalloy disks by excitation of spin waves. In this case, the combination of the spin waves with the dip particle can effect the switching process at lower velocities. In another work [27], a double switching of the magnetic vortex core is shown in simulations of permalloy strips at fields of 0.7 mT, where there is

\*[jab298@case.edu](mailto:jab298@case.edu)

no clear correlation between the velocity of the VC and its switching. Other simulation works predicting reduced critical velocity for reversal include a pac-man-shaped disk [28], application of a perpendicular bias field [29], and an edge-soliton-mediated mechanism [30].

In this study, we experimentally observe deterministic VC switching at  $v_c$  as low as 20 m/s in a standard thin permalloy disk when the VC, undergoing gyrotropic motion, passes through nanoscale localized regions of the material. For comparison, in our system we expect the vortex-antivortex-vortex system to nucleate close to the predicted critical velocity  $v_c \sim 300$  m/s [16–18,20,21,23,31]. We attribute this switching to a local reduction of  $A$  or saturation magnetization  $M_s$  at laser-induced defects. By tuning the excitation pulse and bias magnetic field, we can control the number of switches per pulse from zero up to eight, as well as demonstrate deterministic single-shot switching.

The rest of the manuscript is organized as follows. In Sec. II, we provide background on magnetic vortices and magnetic vortex dynamics, a description of the samples, and the experimental and simulation methods. In Sec. III A, we present experimental results demonstrating repeated VC reversal following prolonged laser exposure. We then show in Sec. III B how VC reversal mainly occurs in regions of the sample with high laser exposure. Single-shot VC reversal is demonstrated in Sec. III C. Finally, in Sec. III D we describe micromagnetic simulations that shed light on possible mechanisms for defect-assisted VC reversal.

## II. SAMPLES AND METHODS

### A. Magnetic vortex and samples

The characteristic magnetic texture in micron-sized soft ferromagnetic disks is a vortex state, in which the magnetization curls around in plane; see Fig. 1(a). However, due to short range exchange interaction, magnetization starts to turn out of the plane at the center of the vortex in a region approximately 10 nm. This region, the vortex core, constitutes a topological defect with polarity  $p = \pm 1$ , either up or down. An in-plane magnetic field sets the VC equilibrium position  $\mathbf{x}_0 \approx \chi_0(B_x, -B_y)$ , with  $\chi_0 \approx 70$  nm/mT here. By applying a fast magnetic field step, the VC undergoes dynamics out of equilibrium, following a gyrating trajectory  $\mathbf{x}(t)$  governed by the Thiele equation [32], eventually spiraling in to the new  $\mathbf{x}_0$  on a tens of nanosecond timescale. The sense of VC gyration, clockwise (CW) or counterclockwise (CCW), is determined by the polarity  $p = \pm 1$  of the VC. Throughout this paper, we consider CW and CCW gyrations as “core down” (shown by solid lines) and “core up” (shown by dashed lines), respectively.

Samples in this experiment are 2.2- $\mu\text{m}$ -diameter, 40-nm-thick permalloy disks, and are fabricated by electron-beam lithography, electron-beam evaporation,

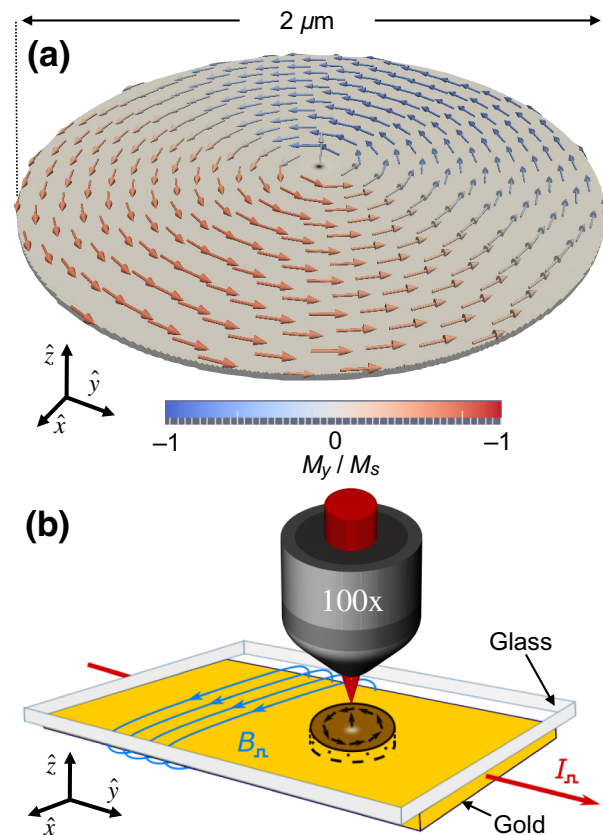


FIG. 1. Samples and the magnetic vortex. (a) A simulated ferromagnetic vortex state with the core polarity up. (b) Schematic of the sample; a permalloy disk (brown) is capped by a gold coplanar waveguide. A microscope objective is used to focus the laser light on the disks.

and liftoff, on a glass coverslip as illustrated in Fig. 1(b). A 120-nm-thick gold coplanar waveguide (CPW) is fabricated on the glass coverslip over the disks. Electrical current pulses  $I_{\parallel}$  through the gold CPW induce in-plane magnetic field pulses  $B_{\parallel}$  in the  $x$  direction at the position of the permalloy disks. A static offset to the stripline current also yields a bias field  $B_0$  in the  $x$  direction. Additionally, an electromagnet provides static magnetic fields in the  $y$  direction.

### B. Experimental method

In order to observe the VC trajectory  $\mathbf{x}(t)$ , we use a three-dimensional (3D) time-resolved magneto-optical Kerr effect (3D TR-MOKE) technique [33]. In this method, a pulsed laser with 5 MHz repetition rate,  $\lambda = 660$  nm, pulse duration approximately 20 ps, and average power of 90  $\mu\text{W}$  before the 100 $\times$  oil-immersion objective lens (numerical aperture  $\text{NA} = 1.25$ ) is focused on the disks after passing through the glass coverslip. The laser spot, with a radius of approximately 200–300 nm, is centered on the VC equilibrium position and any motion of the VC

within the probe spot results in a differential change in the net magnetization under the spot, and is detected as a change in the reflected polarization. In order to observe the gyrations of the VC, we excite the dynamics by 35-ns-duration magnetic field pulses with a variable delay  $\Delta t$  relative to the laser pulses. We measure the equilibrium VC position  $\mathbf{x}_0$  using static MOKE and raster scanning the sample past the probe laser [33].

As we will see below, defects in a ferromagnetic material play an important role in determining VC dynamics. In order to characterize the positions and strengths of these defects, we use the VC as a probe, raster scanning a quasistatic in-plane magnetic field  $B$ , and observing the effect of defects on the vortex equilibrium position  $\mathbf{x}_0$ . When the vortex core becomes pinned at a defect, we observe a plateau in  $\mathbf{x}_0$  versus  $B$ , and often hysteretic  $\mathbf{x}_0$  depending on the sweep direction of  $B$ . The length of the plateaus, the size of jumps in and out of the plateaus, and the degree of hysteresis reveal the spatial extent and strength of the pinning [34]. We use this method to observe the enhancement of pinning due to laser exposure, and correlate it with the observation of VC switching.

### C. Micromagnetic simulations

We perform micromagnetic simulations using an in-house code [35]. We use a disk with a diameter of 1000 nm and a thickness of 40 nm on a regular grid of  $2 \times 2 \times 5 \text{ nm}^3$ . We generally use this disk diameter rather than the 2200 nm of the experimental systems in order to reduce simulation times; in any case, the physical mechanism of core polarity reversal does not depend on the disk diameter so long as it is much larger than both the magnetic exchange length and the disk thickness. The code integrates the Landau-Lifshitz-Gilbert equations

$$\frac{d\hat{\mathbf{m}}}{dt} = -\frac{\gamma}{1+\alpha^2}\hat{\mathbf{m}} \times \mathbf{H}_{\text{eff}} - \frac{\gamma\alpha}{1+\alpha^2}[\hat{\mathbf{m}} \times (\hat{\mathbf{m}} \times \mathbf{H}_{\text{eff}})] \quad (1)$$

with the effective field  $\mathbf{H}_{\text{eff}} = -\delta E/\delta \mathbf{M}$ , where  $E$  is the total energy,  $\mathbf{M}$  the magnetization density, and  $\hat{\mathbf{m}} = \mathbf{M}/|\mathbf{M}|$ . The total energy includes exchange energy, magnetostatic energy, anisotropy energy (here negligible), and Zeeman energy. The magnetostatic field is calculated using the fast Fourier transform, and time integration is done using an implicit adjustable-time Bulirsch-Stoer integrator.

In order to verify that the simulation parameters yield vortex behavior consistent with experimental observation, we first perform quasistatic simulations of disks in an in-plane magnetic field of 2.5–5.0 mT and calculate the displacement of the vortex core using a Gilbert damping of  $\alpha = 0.2$ . For a disk of diameter 2000 nm and magnetic parameters  $A = 13 \text{ pJ/m}$  and a magnetization density of  $M = 8.00 \times 10^5 \text{ A/m}$ , we obtain a core displacement of about 52 nm/mT, and for a diameter of 1000 nm, we obtain about 14 nm/mT, which are in reasonable range of

published values [36]; for a 2200 nm diameter disk 40 nm thick with  $M = 7.80 \times 10^5$  ( $7.00 \times 10^5$ ) A/m and a  $2 \times 2 \times 10 \text{ nm}^3$  mesh, we obtain a displacement of 64 (72) nm/mT. The experimentally estimated displacement susceptibilities are 66–76 nm/mT, and we therefore generally reduce the magnetization density to  $7.00 \times 10^5 \text{ A/m}$  in our simulations. The exchange coupling is less important for the core displacement as it is primarily driven by magneto-static interactions, and in the simulations we use values of  $A = 10 \text{ pJ/m}$  and  $A = 13 \text{ pJ/m}$ .

In order to simulate dynamical core reversal, we create the two defect configurations described below. We then initialize the system with a vortex with a core located away from the defect region and time integrate the magnetization evolution in time steps of 0.1 ps with a Gilbert damping of  $\alpha = 0.01$ . We also perform some checks that the reduction of the magnetization density does not appreciably change our conclusions by running simulations with  $M = 7.00 \times 10^5 \text{ A/m}$  in the defect region. Finally, we also check that the initial core polarity does not alter our conclusions by running simulations reversing the initial polarity.

## III. RESULTS

### A. Experimental observations of VC reversal

We now compare the VC gyrations before and after prolonged exposure of the pulsed laser, starting from different  $\mathbf{x}_0$ . We demonstrate that after extended laser exposure, VC reversal occurs at multiple spots. Figures 2(a) and 2(b) show the VC gyrations in response to a 35 ns magnetic pulse before and after prolonged laser exposure time. In Fig. 2(a), the scan begins before the pulse ( $\Delta t < 0$ ) when  $\mathbf{x}(t) = \mathbf{x}_0$ . During the pulse, we observe gyrations about  $\mathbf{x}_1$ . By the end of the pulse, the VC has partially relaxed to  $\mathbf{x}_1$ . After the pulse, the VC again undergoes gyrations as it relaxes back to  $\mathbf{x}_0$ . The sense of the gyrations is CCW everywhere (indicated by dashed lines), indicating a constant VC polarity with no polarity switch.

After further exposure to the pulsed laser (approximately 6 h) focused to a several hundred nanometer spot on the disk center, we observe significantly altered gyrations [Fig. 2(b)]. During the pulse, we observe CCW gyrations about  $\mathbf{x}_1$ . Then, as the VC approaches  $(x, y) = (-32, -155) \text{ nm}$ , the gyration switches to CW, indicating a core polarity switch. After the pulse ends, the VC begins relaxing to  $\mathbf{x}_0$ , still with CW gyrations until it hits another switching spot near  $(x, y) = (5, 90) \text{ nm}$  and suddenly reverses direction. As the VC continues to relax back to the center, we observe another seven switching spots, indicated by red arrows. Because of the stroboscopic nature of the experiment, each data point in the scan is an average of approximately  $10^6$  repetitions of  $\mathbf{x}(t)$ , indicating the deterministic nature of the trajectory, and the entire

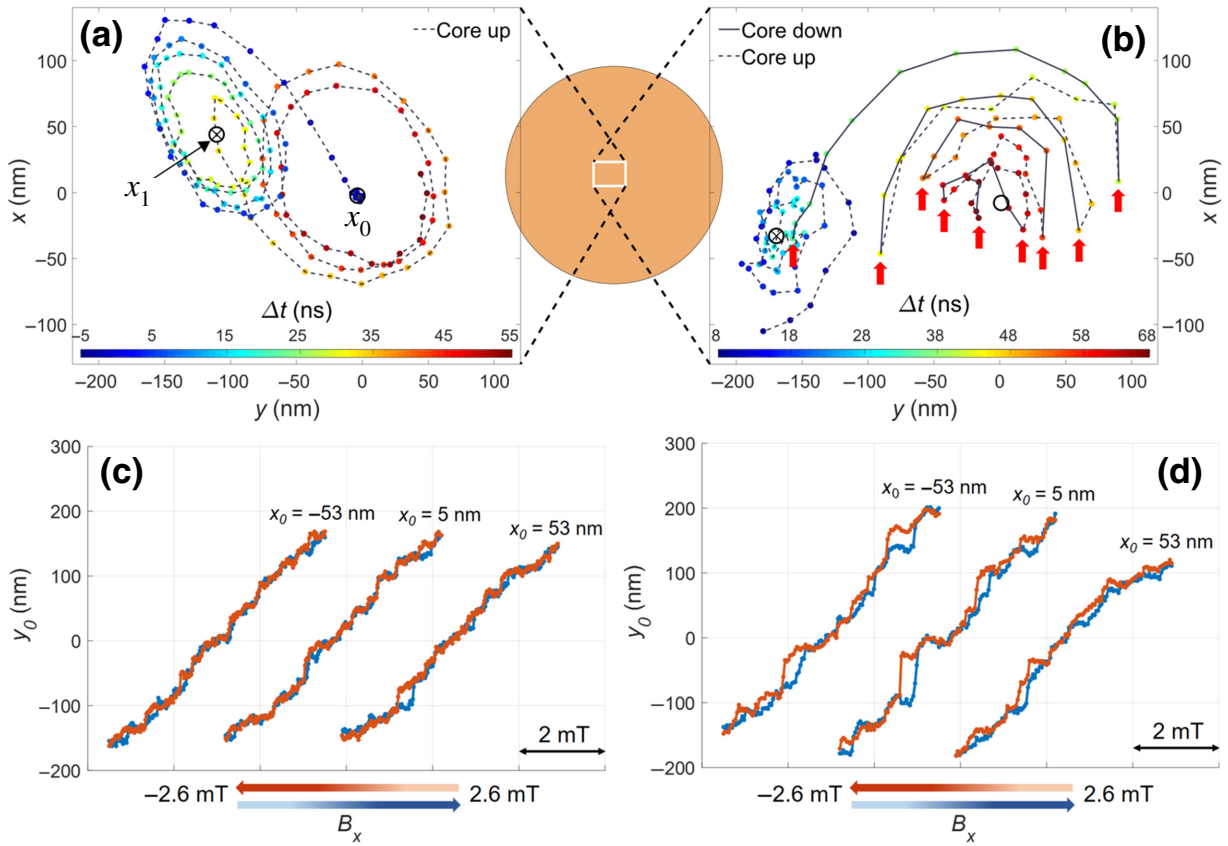


FIG. 2. Magnetic vortex core reversal by defects. (a),(b) Gyration of the VC before and after prolonged pulsed laser exposure. The color bar  $\Delta t$  indicates the time relative to the beginning of the pulse. Each red arrow represents a VC reversal. The VC velocity is shown by the values under each red arrow, which is an average velocity of the VC (m/s) on each arc before reversal, with an error of approximately 6 m/s. (c),(d) The VC equilibrium position  $y_0$  versus  $B_x$  swept up (blue) and down (red) at three different values of  $x_0$  before and after the laser exposure, respectively.

scan is taken multiple times to check the reproducibility of the measurement.

The VC velocity in m/s preceding each reversal is shown below each red arrow in Fig. 2(b). These values are calculated based on the time and path length since the previous switch (and averaged over several points in the case of the first switch). The error in VC velocities is approximately 6 m/s, which is calculated based on the error in time (here small) and signal fluctuations in all  $x$  and  $y$  coordinates of the VC on each arc before reversal. Previous work has found that a critical VC velocity  $v_c \approx 300$  m/s is necessary to switch the polarity in permalloy disks under these conditions [16–18,20,21,23,31]. However, in Fig. 2(b), we observe VC reversal at velocities as low as  $v_c \approx 20$  m/s. To understand how the laser has changed the defect landscape, we look at the  $y_0$  versus  $B_x$  hysteresis loops at different values of  $x_0$  (different  $B_y$ ) before and after prolonged exposure. In the absence of any defects, we expect a linear  $y_0 = \chi_0 B_x$ . However, defects likely associated with grain boundaries or other structural inhomogeneities cause the plateaus, jumps, and hysteresis seen in Figs. 2(c) and 2(d) [34,37]. Figure 2(c) shows three

hysteresis loops on the same sample before the prolonged exposure, offset horizontally for clarity. In these hysteresis loops, localized intrinsic defects created during the fabrication process cause small plateaus to appear with some hysteresis visible. Figure 2(d) shows the same measurement after approximately 13 h of exposure to the pulsed laser, following both the measurements shown in Figs. 2(b) and 3. Clearly, we now observe more prominent plateaus, jumps, and hysteresis. We hypothesize that water or oxygen is trapped between the permalloy and the gold cap during the separate fabrication steps, which then undergoes laser-assisted diffusion into existing grain boundaries, resulting in local reductions in  $A$  and/or  $M_s$  [38–41].

## B. Translating the VC trajectories

Additional insight into the VC reversal mechanism is gained by translating the region of the VC dynamics away from the disk center using a bias field  $B_0$ . We will see that the switching occurs mainly near the center of disk. Vortex dynamics away from the center show little to no switching. In Fig. 3, we show additional measurements at different

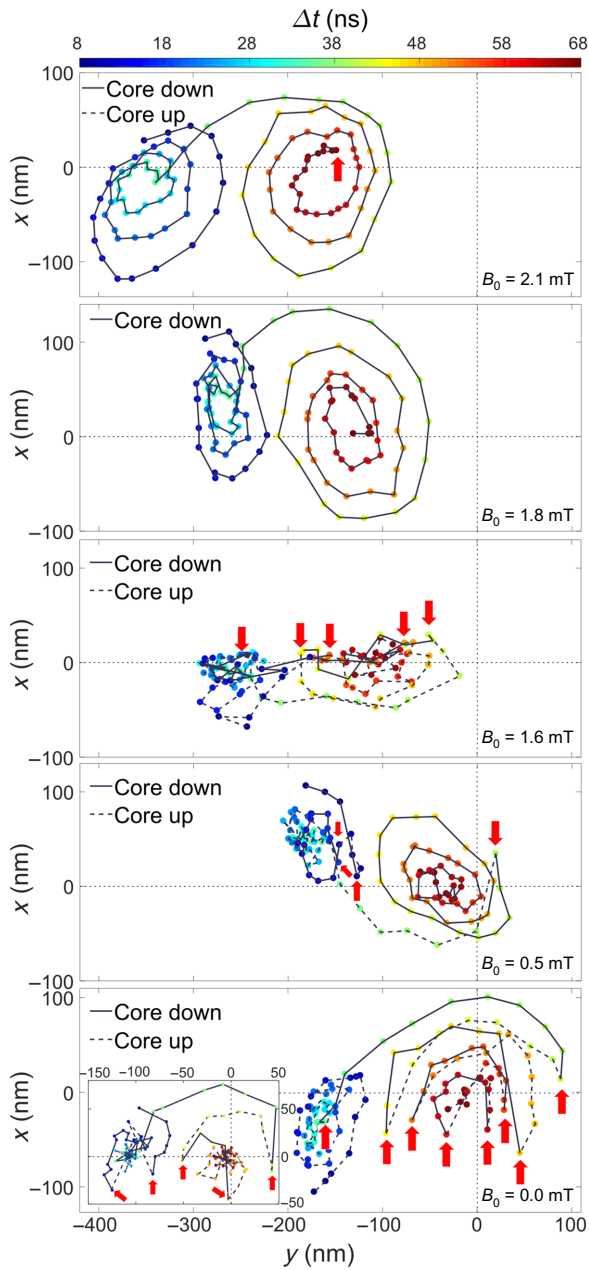


FIG. 3. From top to bottom: 2D TR MOKE of magnetization dynamics as we shift the VC from the left region towards the center. In all cases except the inset in the bottom panel we use a 3.2 mT amplitude, 35 ns magnetic field pulse. We use fixed biased fields ( $B_0$ ) along  $+\hat{x}$  to shift the VC from the left (top panel) towards the center (bottom panel). Color bars  $\Delta t$  indicate the time relative to the beginning of the pulse. Inset in the bottom panel shows the gyrations of the VC near the center excited by a smaller magnetic pulse of 1.6 mT. VC reversals are indicated by red arrows.

static bias fields  $B_0$  along the  $x$  direction as the trajectory is translated away from to the center of the disk in the  $y$  direction.

These measurements are all taken after the scan shown in Fig. 2(b), where repeated switching is observed

following approximately 6 h of pulsed laser exposure. The order in which the scans are taken is  $B_0 = (0, 2.1, 1.6, 1.8, 0.5)$  mT, with approximately 1 h of cumulative laser exposure between scans. The fact that the scans are not taken in order from top to bottom indicates that the observed trends are not due to cumulative laser exposure.

The top panel shows the largest offset  $B_0 = 2.1$  mT, and little to no switching is observed. Note that this scan is taken after Fig. 2(b) and the bottom panel of Fig. 3, in which multiple switches occurred near the center of the disk. This demonstrates that the switching behavior is mainly limited to the center of the disk, where laser exposure is greatest. The second panel shows the trajectory shifted slightly to the right, but still with little to no switching observed. The change in shape of the gyrations may be an artifact due to alignment of the probe laser. (If the VC moves toward the edge of the probe laser spot, the measured signal is less sensitive to VC displacement, resulting in a flattening of the measured displacement.) The third panel shows an intermediate regime where we believe the switching is not deterministic, discussed further below. Here we see a partial cancellation of the motion in the  $x$  direction. Moving further towards the center, the fourth panel shows clear gyrations again, now with several switches visible. Finally, the bottom panel shows similar data as in Fig. 2(b), with multiple VC reversals. The inset in the bottom panel demonstrates switching at a lower pulse amplitude of 1.6 mT. Here, we use no offset field, and the pulse duration is 35 ns. In this figure, there are at least three switching spots. Most clearly, switching can be seen near  $(x, y) = (0, \pm 50)$  nm when the VC starts to relax back to the center. It is possible that switching may be possible at still lower pulse fields, though the signal becomes increasingly difficult to discern above the noise.

These results provide strong evidence for the hypothesis that the VC reversal seen here is caused by defects. In the first measurements on a pristine sample using the experimental parameters described here, we observe no VC reversal. But after prolonged laser exposure, we begin to observe VC reversal using the same experimental parameters. This implies that the sample must have changed during this time period. And even then, VC reversal is only seen in the region of the sample with the greatest laser exposure. Furthermore, the regions with larger laser exposure are observed to have enhanced vortex pinning, indicating the strengthening of the disorder in those regions.

We further investigate the region of  $B_0$  seen in the third panel of Fig. 3 (at  $B_0 = 1.6$  mT) attributed to stochastic switching. By “stochastic” we mean that different numbers of switching events occur at random for subsequent repetitions of the magnetic field pulse. This is in contrast to the deterministic switching shown above, in which many repetitions of the magnetic field pulse yield consistent

switching behavior. We would expect this to occur in an intermediate regime where the VC trajectory is on the cusp of transitioning from a region with no reversal to a region with reversal. In this regime, fluctuations from electrical or thermal noise can strongly affect the success or failure of switching.

In Fig. 4, we show the trajectory at  $B_0 = 0.6$  mT (in between the third and fourth panels of Fig. 3). The left panel shows the trajectory in 2D, with  $x(t)$  and  $y(t)$  plotted separately on the right. In the region close to the center of the sample where switching normally occurs (labeled “Mixed”), we still see oscillations in the  $y$  component, but mainly noise in the  $x$  component. This is to be expected if the number of VC reversals varies stochastically from one magnetic field pulse to the next. Regardless of the sense of gyration (CW or CCW) the trajectory component  $y(t)$  is unchanged, and therefore still shows clear oscillations. However, the  $x$  component will be reversed if the sense of gyration is reversed. For example, at the moment the pulse is turned off and the VC is at a position  $y < 0$ , we would expect motion in the positive  $x$  direction for CW motion and motion in the negative  $x$  direction for CCW direction. Yet both CW and CCW motion would result in motion in the positive  $y$  direction. Therefore, if the number of switches varies from one pulse to the next, we expect the  $x$  component to average to zero, but the  $y$  component to still display clear oscillations. Note that the oscillations are still visible in all components in the dynamics during the pulse ( $\Delta t < 35$  ns). This is expected if no stochastic switching occurs in this region, though it also requires that the VC begins with some preferred polarity. We believe that this region of nondeterministic switching occurs as the VC is in between regions of no switching and deterministic switching, and thermal or electronic noise is sufficient to cause some of the VC reversals to either occur or not from one repetition to the next.

### C. Reliability of VC reversal by defects

For data storage applications, we require a single-shot switch with high reliability. To demonstrate single-shot switching, we start from a new sample with no observed switching [Fig. 5(a)]. We then expose the sample to the pulsed laser, while repeatedly measuring the VC trajectory until we observe switching events begin to appear. Finally, we observe a switching spot  $\mathbf{x}_{sw}$  shown with a red arrow in Fig. 5(b). We use this switching spot for the single-shot switching and to further test the reliability of VC reversal in this method.

Figure 5(b) illustrates a protocol for single-shot switching and subsequent polarity measurement. First, a single 5-ns-duration magnetic field pulse drives half a period of gyrotropic motion (green) from the initial equilibrium position  $\mathbf{x}_0$  towards the single switching site ( $\mathbf{x}_{sw}$ ). The VC then relaxes back to  $\mathbf{x}_0$ . Next the VC is adiabatically translated (purple) to another position where clear gyrations with no switching are observed (blue). The sense of these gyrations indicate the VC polarity. A short TR-MOKE scan about this new equilibrium then reveals the VC polarity, as shown in Figs. 5(c) and 5(d). The scans in Figs. 5(c) and 5(d) are obtained with significantly more averaging, so as to reduce the noise for demonstration purposes; in practice, faster scans suffice to determine the gyration direction. Note that in this single-shot switching experiment, there is no laser excitation during the VC reversal protocol. This demonstrates that the probe laser pulse is not playing a role in the reversal dynamics.

Figure 5(e), from top to bottom, demonstrates the VC polarities after applying single sequential 5 ns magnetic field pulses. Each core polarity up (down) is represented by a red up (blue down) arrow. Above each arrow, a green check mark indicates a successful switch. Failed switches are represented by a red cross. The polarity starts out up. Following one single-shot pulse, the polarity has flipped to

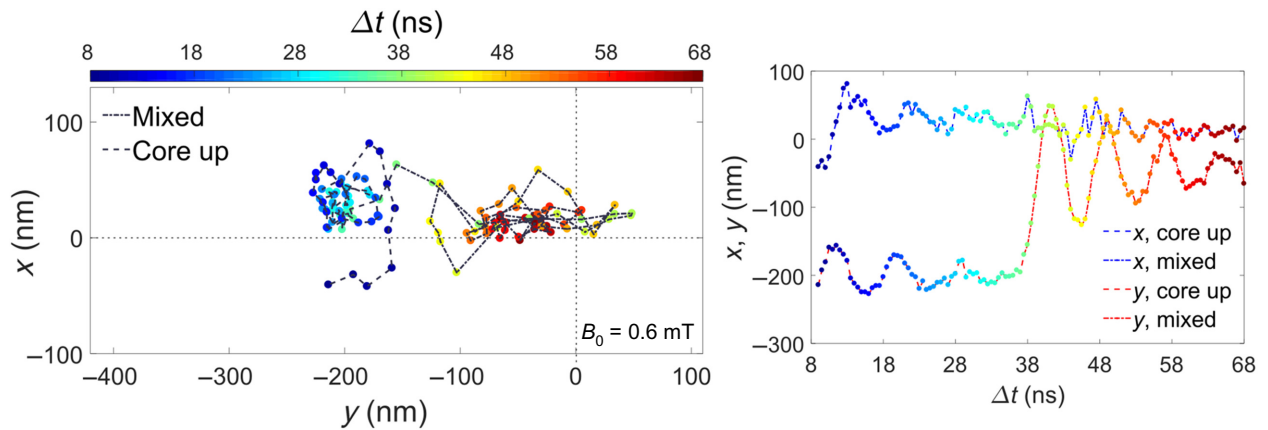


FIG. 4. Region of stochastic switching (sample 1). The left panel demonstrates the 2D gyrations of the VC at  $B_0 = 0.6$  mT. The  $x$  and  $y$  components are shown separately versus time on the right. To excite these gyrations, a 3.2 mT amplitude and 35 ns magnetic pulse is used. Color bar  $\Delta t$  indicates the time relative to the beginning of the pulse.

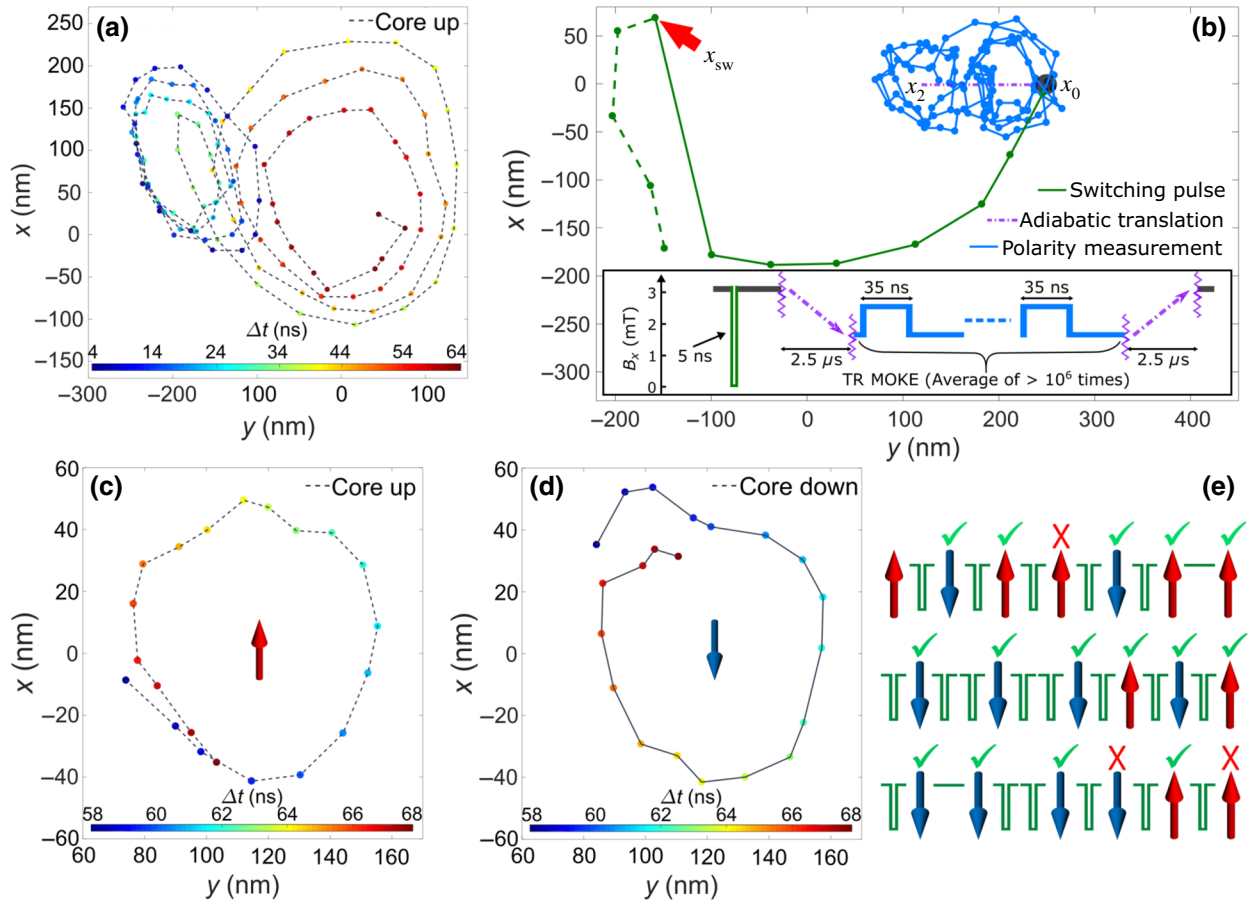


FIG. 5. Single-shot switching. (a) Normal gyrations on disk 2 before the prolonged pulsed laser exposure. (b) Schematic of the procedure used to switch and test the polarity. Red arrow indicates the reversal spot appearing after pulsed laser exposure. (c),(d) Examples of VC dynamics used to respectively measure core polarities up and down after a single-shot switch. (e) Core polarities before and after each switching pulse. Green check marks (red cross) above each core polarity illustrate the successful (failed) switches. The color bars  $\Delta t$  show the time relative to the beginning of the 35 ns pulse.

down. This pattern repeats, and we verify that the polarity does not flip with no pulse, and flips twice with two pulses. From eighteen tests in this process, fifteen of them are successful. We believe the last two failures are due to further laser-induced enhancement of the defect after approximately 1 h of measurement time.

#### D. Simulation results

In order to gain insight into the mechanisms for the switching observed here, we simulate the interaction of the vortex core with a pinning site modeled as a localized region of reduced exchange constant  $A$  and/or saturation magnetization  $M_s$  (see the Supplemental Material [42] for simulation movies).

We begin by simulating the equilibrium displacement of the VC versus applied field as the VC traverses a defect region, to verify that defect areas in which the exchange coupling has been reduced, e.g., by diffusion of oxygen or other defects from the Py-Au interface, can give rise to the

observed hysteresis and core polarity reversal. We first create a “defect region” of radius 15 nm centered 115 nm from the disk center along the  $y$  axis. In this region, we reduce the exchange coupling  $A$  from  $A = 13$  pJ/m in the disk to values ranging from 1.3 to 10 pJ/m, and for each value of the exchange coupling, simulate the quasistatic trajectory of the vortex core in applied fields from 0 to 15 mT and then back to 0 mT along the  $x$  axis. Traces of the simulated VC displacement  $y_0$  versus static field  $B_x$  swept up and down are shown in Fig. 6. At  $A = 10$  pJ/m, there is a small onset of hysteresis visible, and at  $A = 2.5$  pJ/m the hysteresis is quite large. The core is deformed and deflected by the defect region towards negative  $x$  with increasing field, and towards positive  $x$  with decreasing field (not shown in the figure). At the lowest value of  $A$ , 1.3 pJ/m, the lateral deflection is about 27 nm, while for  $A = 10$  pJ/m, the deflection is only about 5 nm with no clear deformation of the core. See Movie S1 within the Supplemental Material [42] for a video of the quasistatic hysteretic behavior of the VC position. As  $A$  is reduced, we observe the emergence

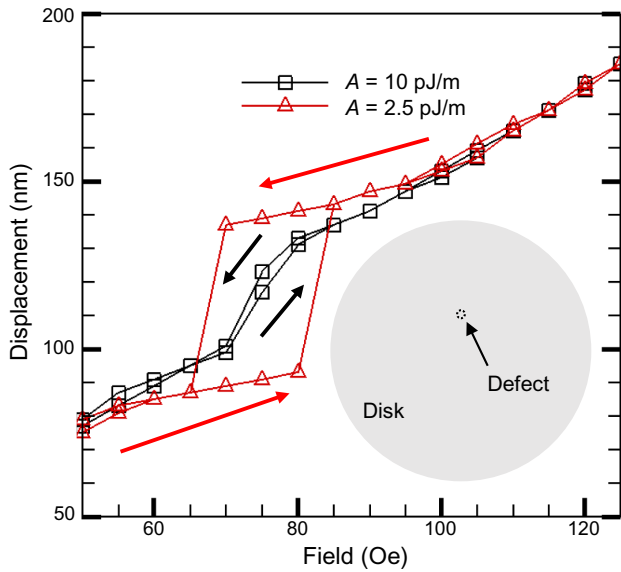


FIG. 6. VC equilibrium position  $y_0$  versus  $B_x$  swept up and down. Pinning and hysteresis occur as the VC traverses a 30-nm diameter region where the exchange coupling is reduced to 10 pJ/m (black squares) and to 2.5 pJ/m (red triangles) from the nominal value of 13 pJ/mm. Red (black) arrows show the direction of the field sweep for red (black) hysteresis.

of similar pinning and hysteresis as seen in the experiment following prolonged laser exposure [Figs. 2(c) and 2(d)]. This demonstrates that this type of defect is consistent with those seen in the experiment.

We then simulate the nonequilibrium vortex dynamics with a trajectory passing through a defect region. It is difficult to implement some disorder or defects that are a faithful representation of the disorder in the experimental system. For example, earlier work [36] has shown that defect sizes and morphology inferred from vortex oscillations do not correlate with grain structure as observed using microscopies. Therefore, we focus the simulations on proof of concepts to demonstrate that the kind of defects we think are most likely to be induced, reduced exchange coupling and/or magnetization density, can lead to a significant reduction in the critical velocity for core reversal, consistent with the experimental observations. Specifically, we simulate the VC dynamics in two geometries. First, we reduce  $A$  along a strip of the disk extending from  $x = 0$  to 100 nm. In this strip,  $A$  is reduced to 2 from 10 pJ/m elsewhere on the disk. This is intended to capture an extended defect cause by a grain boundary or crack in the sample. Next we add a  $10 \times 10$  nm<sup>2</sup> nonmagnetic region within the strip of reduced  $A$ . This configuration is meant to capture the effect of a pointlike defect along the linear defect. In general, there are many possible defect configurations. The two we describe below, however, provide evidence that these types of defect can reproduce the experimentally observed VC reversal.

In the reduced- $A$  strip simulation, we observe two VC reversals (see Movies S2, S4, and S5 within the Supplemental Material [42]). Figure 7(a) plots the simulated trajectory of the VC. Points within the reduced- $A$  strip are circled in red. The VC is initially gyrating in the CW direction, then immediately reverses to CCW upon reaching the defect strip. The trajectory then continues in the CCW direction until encountering the defect strip again. After briefly entering the defect strip, the gyration again changes direction. Subsequent encounters with the defect strip do not cause reversal. The fact that the reversal occurs within the first 10 nm of the strip suggests that a narrower extended defect would also cause reversal.

The speed  $v$  of the VC as it undergoes the trajectory in Fig. 7(a) is shown in Fig. 7(b). Vertical lines at each point indicate numerical noise due to the  $2 \times 2$  nm<sup>2</sup> simulation grid. Data points have been removed near the reversal points where the VC position is not well defined or where higher temporal resolution is required to resolve the instantaneous velocity. As such, the main panels serve to indicate approximate VC speeds on the gyrotropic trajectories in between reversals. The insets show the indicated time spans with higher temporal resolution, and higher spatial resolution by interpolating the VC position. Note that  $v$  is generally less than the  $v_c \approx 300$  m/s expected for a pristine disk, so we do not expect VC reversal here in the absence of defects. As the VC approaches the defect strip, the VC trajectory is significantly altered, resulting in large swings of the instantaneous speed (see the inset), and a significant reduction of  $v$  after passing through the defect region. The two red arrows in Fig. 7(b) indicate the VC reversals. The first reversal occurs very rapidly after the VC enters the defect strip when  $v \approx 150$ –250 m/s, and the second reversal occurs somewhat later after entering the defect strip when  $v \approx 150$  m/s. These values of  $v$  are approximated from the values for the VC outside of the defect region on either side of the reversal. Within the defect region during the reversal process, it is difficult to define a single value of  $v$  and even to identify the position of the VC. The VC next encounters the defect region when  $v \approx 100$  m/s, and no reversal occurs. While the two observed reversals occurred at VC speeds well below the critical velocity, the speed is still not as low as the lowest speeds at which VC reversal is observed in the experiments.

Next we add a  $10 \times 10$  nm<sup>2</sup> nonmagnetic region to the defect strip, as indicated in Fig. 7(c), resulting in the trajectory as shown (see also Movies S3 and S6 within the Supplemental Material [42]). The corresponding plot of  $v$  versus  $t$  is shown in Fig. 7(d). Beginning near  $y = -100$  nm, we first see a VC reversal similar to those seen with the reduced- $A$  strip alone with  $v \approx 120$  m/s. When the VC next enters the defect strip with an approximate speed  $v \approx 100$  m/s, no reversal occurs. However, once the VC approaches the nonmagnetic defect, its speed is first further reduced to about 60 m/s [inset to Fig. 7(d)]

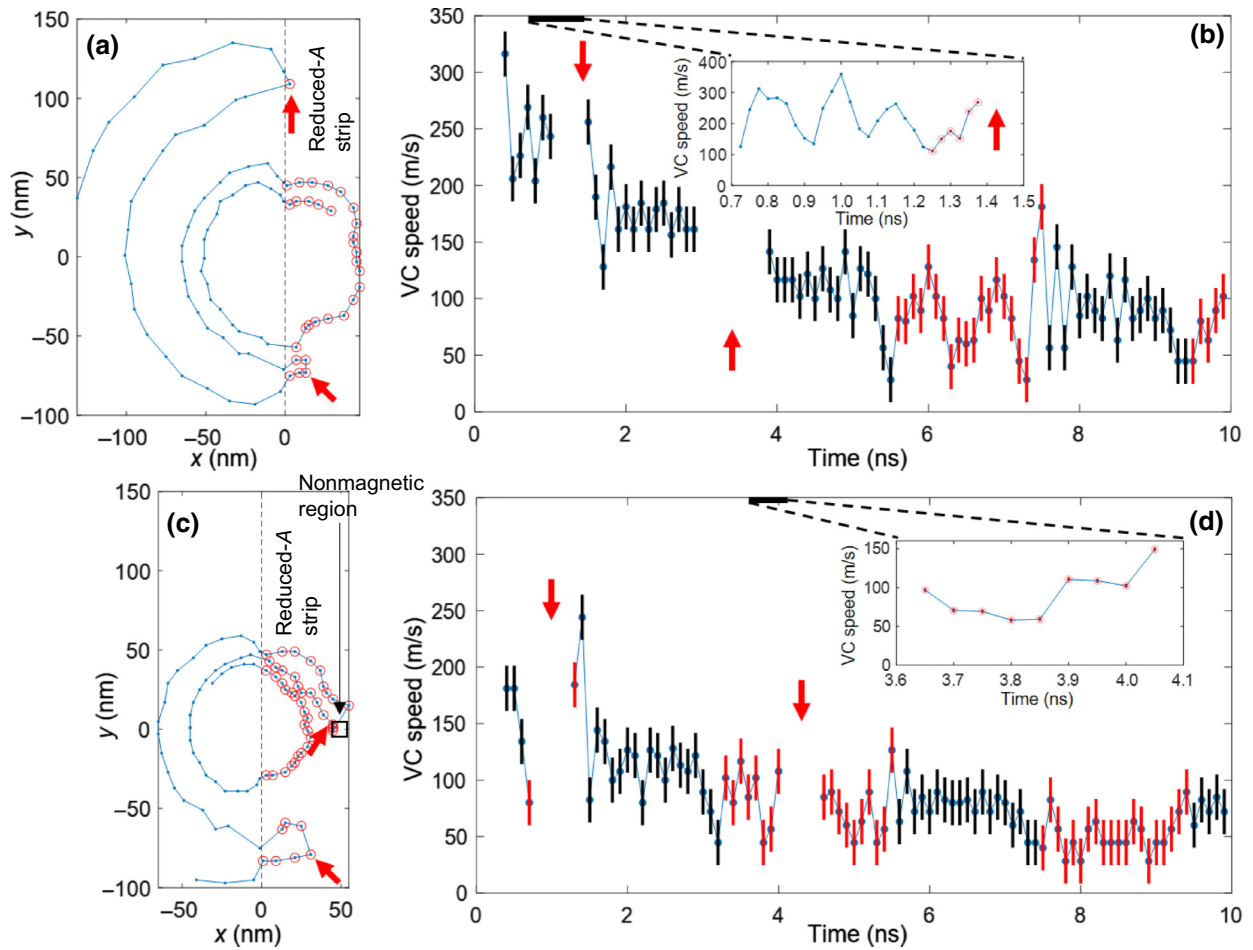


FIG. 7. Simulated VC trajectories. (a) VC gyrotropic trajectory with a defect strip from  $x = 0$  to  $100$  nm where  $A$  is reduced to  $2$  from  $10$  pJ/m. Points are separated by  $0.1$  ns. Points within the defect region are circled in red. (b) Approximate VC speed versus time calculated from (a). Points where the VC is within the defect strip are circled in red. VC reversals are indicated by red arrows. Inset shows the VC speed near the first reversal in panel (a) based on simulations with higher temporal resolution. The VC speed oscillates with an average of about  $200$  m/s and a lowest speed approximately  $120$  m/s before the VC enters the defect region. (c) Same as (a), but showing a smaller amplitude trajectory with the addition of a  $10 \times 10$  nm<sup>2</sup> nonmagnetic region, indicated by the black square; (d) is same as (b), but for the trajectory shown in (c). Inset shows the approximate VC speed based on higher temporal resolution before the core is absorbed by the nonmagnetic defect in panel (d). Within the defect region with lower  $A$ , the VC speed is reduced to about  $60$  m/s before the VC accelerates as it approaches the nonmagnetic defect.

before it accelerates just before the VC is absorbed by the defect and subsequently reversed. These results indicate that reversal can occur at pointlike defects at still lower values of  $v$  than seen with the strip alone. These results are similar to simulations that have studied VC reversal at holes [43].

To understand the VC reversal process seen in the simulations, we can look at a series of snapshots of the magnetization texture shown in Fig. 8. Of the simulated switching events described above, there are two distinct mechanisms shown in Figs. 8(a) and 8(b). First, a VC reversal from the reduced- $A$  strip alone is shown in Fig. 8(a) [corresponding to the first reversal in Fig. 7(a)]. The dashed line indicates the boundary of the reduced- $A$  region at  $x > 0$ . The black

dots show the position of the vortex core at  $25$  ps intervals. No dots are shown during the reversal process itself, when there is no single well-defined VC position. The VC is initially polarized in the negative direction (blue). Panel (i) of Fig. 8(a) shows the VC as it has just traveled from the left, and is about to enter the reduced- $A$  strip. The red wake or dip particle can be seen below and to the left of the VC. After the VC has entered the reduced- $A$  strip [panel (ii)], the wake has significantly increased in magnitude at the defect strip boundary. In panel (iii) the wake has split into a vortex and antivortex, both with positive polarization. In panel (iv), the red antivortex and the original blue VC have annihilated and the reversed VC is now moving to the left. This is essentially the same process

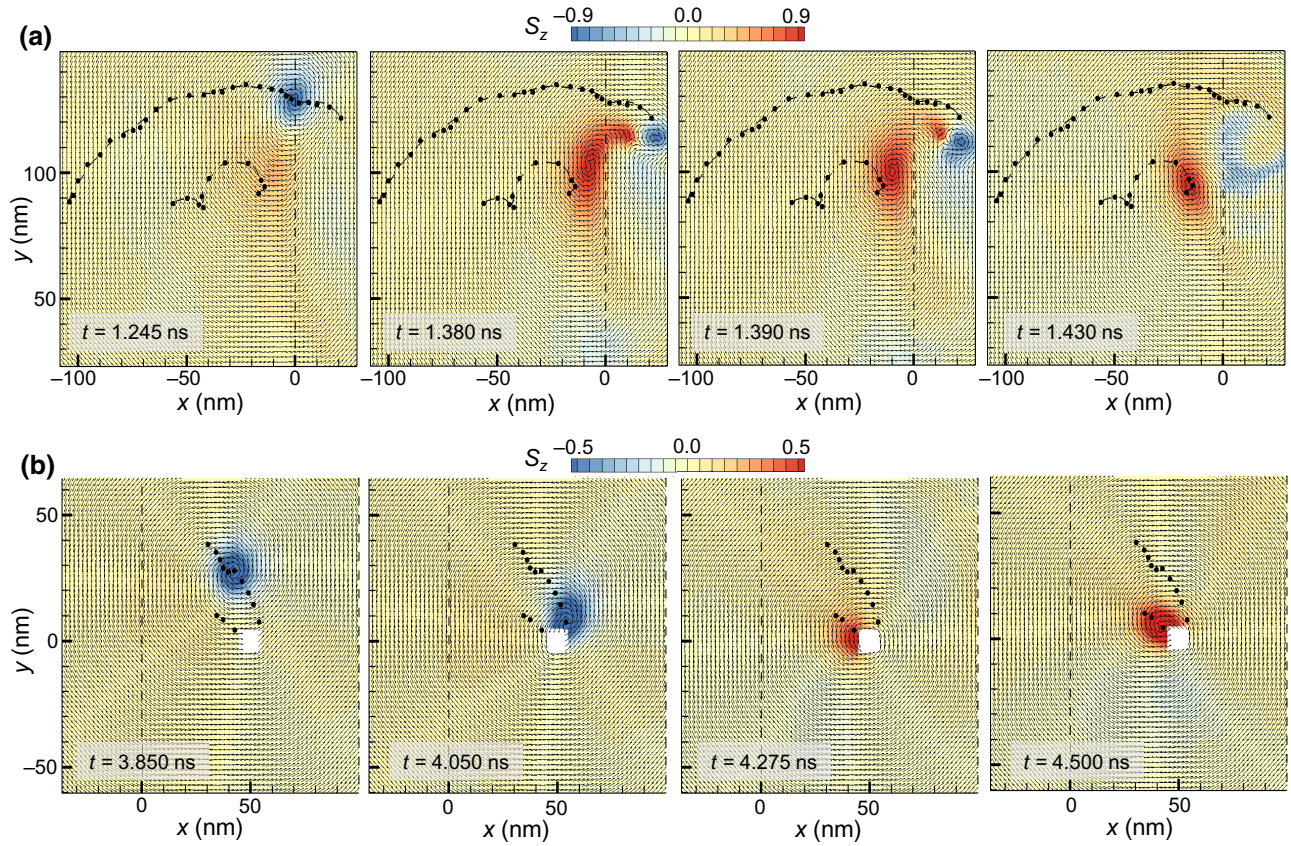


FIG. 8. Snapshots of VC reversal mechanisms. (a) VC reversal at the boundary of the reduced- $A$  strip at  $x > 0$ . Black dots indicate the path of the VC at time steps of 25 ps, starting from  $x \approx -100$  nm. Dots are not shown when no single well-defined VC exists. (i) Negative-polarity VC is just entering the defect strip. (ii) Red wake has deepened, and started to form a positive-polarity vortex-antivortex pair. (iii) Positive polarity VC has formed outside the defect strip, with positive-polarity antivortex adjacent to the original negative-polarity VC. (iv) Original VC has annihilated with antivortex, and new positive-polarity VC is traveling to the left. (b) VC reversal at a nonmagnetic region (white square). Here black dots are separated by 50 ps, indicating lower VC velocity. (i) The VC is traveling CW with a velocity too low to have reversed upon entering the reduced- $A$  region. (ii) The VC begins to be trapped by the nonmagnetic defect. (iii) The VC itself has annihilated on the defect, and the surrounding out-of-plane magnetization has switched to the positive direction. (iv) The VC has reformed with positive polarity and leaves the defect on a CCW trajectory.

as occurs in VC reversal by exceeding  $v_c$ . Since theory predicts  $v_c \propto \sqrt{A}$ , we expect a reduction of a factor of  $\sqrt{5}$  to  $v_c \approx 130$  m/s, consistent with the simulation result. Beyond this, the defect boundary may play a role in the reversal process. As the VC enters the defect region, the trajectory is altered, including sudden changes in velocity that may assist VC reversal. In Fig. 8(a), the original VC enters the defect region, and the antivortex nucleates within the defect region, but the new VC remains outside the defect region, suggesting that the defect boundary may contribute to the nucleation of the vortex-antivortex pair.

The VC reversal process at the pointlike nonmagnetic defect is shown in Fig. 8(b) [corresponding to the second VC reversal in Fig. 7(d)]. Again, the dashed line indicates the boundary of the reduced- $A$  region at  $x > 0$ , and the nonmagnetic region is indicated by the white square. The black dots indicating the VC trajectory are now spaced by 50 ps. The VC begins with negative polarization (blue)

above the nonmagnetic region, traveling CW [panel (i)]. The vortex core becomes trapped by the pointlike defect, and the VC itself is annihilated at the hole, leaving only the negatively polarized region surrounding the core. This surrounding region then rotates to positive polarization (red) in panel (iii). Finally, a reversed VC reforms and unpins from the nonmagnetic region [panel (iv)], then moving along a CCW trajectory. The reversal process is assisted by emission of spin waves as the VC approaches the nonmagnetic defect. The spin waves can be discerned in Fig. 8(b) panels (ii) and (iii) with primarily blue shading. These spin waves carry away negative out-of-plane VC magnetization while the VC is temporarily bound to the defect, which allows for the VC polarity reversal. This reversal process is similar to that explored in simulations of VC reversal by a hole in Ref. [43], but our simulations show that this kind of structure can lead to VC reversal much below the nominal critical speed.

The micromagnetic simulations support the hypothesis that defects serve as localized sites for rapid VC reversal with a significantly reduced critical velocity. The pattern of repeated reversals observed in the experiment suggest that these defects have an extended structure, such as those due to grain boundaries which may have been enhanced due to strain during fabrication or mounting.

#### IV. CONCLUSIONS

Topology can lead to high stability of protected quantities because of the finite energy barrier that needs to be overcome when such topological quantities are changed, for example, switching vortex core polarity or changing skyrmion numbers. However, this stability is also an impediment for exploiting topologically protected quantities in applications that rely on changing such quantities at will. Here we have shown that the polarity of magnetic vortices, which is topologically protected, can be switched deterministically without the application of large external magnetic fields by introducing local defects in a magnetic material through laser illumination.

The defects enable vortex core polarity switching by reducing the critical velocity by over an order of magnitude. This is significant, because the VC velocity preceding a switch is a measure of the magnitude of excitation that must be applied. When the VC enters a region with reduced exchange coupling  $A$  such that the VC speed exceeds the critical velocity  $v_c$ , the wake pool or dip deepens and creates a vortex-antivortex pair with the core of the vortex having reversed polarity compared to the original VC. The original VC then annihilates with the antivortex, and a VC with reversed polarity continues [Fig. 8(a)].

The simulations also show that the discontinuity in exchange coupling gives rise to a distorted wake pool, while the deepened wake enters the defect region and eventually annihilates the original VC. The discontinuity also gives rise to long-range magnetostatic interactions driven by the VC dynamics, which cause fluctuations in the VC speed even in defect-free regions, possibly assisting VC reversal as in previously observed spin-wave-assisted reversal [26].

In the presence of the nonmagnetic defect [Fig. 8(b)], the reversal process is different: as the core approaches the defect, out-of-plane fluctuations of the magnetization density increase (spin waves). This can be seen in Movie S6 within the Supplemental Material [42] where the out-of-plane magnetization is color coded, and can also be discerned in the last two panels of Fig. 8(b). The out-of-plane fluctuations cause the core to reemerge but with opposite polarity and lower energy of the vortex. The excess energy has been dissipated by spin waves that also carried away the excess or difference in out-of-plane magnetization density from the vortex core. Note that if the defect is too large, it simply binds the core without

emitting a core with reversed polarity. This reversal mechanism was observed in Ref. [43] and is different from the reversal without defects when the core exceeds the critical velocity. We have shown that VC reversal primarily occurs in regions of the sample with the highest pulsed laser exposure. The switching can therefore be controlled by translating the VC to regions of the sample with more or fewer switching sites. In future work, it will be important to understand how different types of defects lead to switching behavior, and how such defects may be engineered with finer control, such as through nanolithography or ion milling. This points to a direction for realizing applications such as memories or logic devices in which it will be important to control the vortex core polarity switching either to suppress bit-flip errors, or to engineer local sites for fast, reliable switching.

#### ACKNOWLEDGMENTS

O.H. acknowledges funding from the US Department of Energy, Office of Science, Basic Energy Sciences Division of Materials Sciences and Engineering. We gratefully acknowledge the computing resources provided on Bebop and Blues, high-performance computing clusters operated by the Laboratory Computing Resource Center at Argonne National Laboratory. M.M. proposed the idea of reversal at defects, constructed the apparatus, and carried out the experiment, J.B. advised on the sample fabrication and experiment, and O.H. performed micromagnetic simulations. M.M., J.B., and O.H. participated in data analysis and editing the manuscript. J.T. fabricated samples.

- 
- [1] T. Okuno, K. Shigeto, T. Ono, K. Mibu, and T. Shinjo, MFM study of magnetic vortex cores in circular permalloy dots: Behavior in external field, *J. Magn. Magn. Mater.* **240**, 1 (2002).
  - [2] S. S. Parkin, M. Hayashi, and L. Thomas, Magnetic domain-wall racetrack memory, *Science* **320**, 190 (2008).
  - [3] A. Fert, V. Cros, and J. Sampaio, Skyrmions on the track, *Nat. Nanotechnol.* **8**, 152 (2013).
  - [4] A. Fert, N. Reyren, and V. Cros, Magnetic skyrmions: Advances in physics and potential applications, *Nat. Rev. Mater.* **2**, 17031 (2017).
  - [5] J. Zang, V. Cros, and A. Hoffmann, *Topology in Magnetism* Vol. 192 (Springer, Cham, 2018).
  - [6] L. D. Geng and Y. M. Jin, Magnetic vortex racetrack memory, *J. Magn. Magn. Mater.* **423**, 84 (2017).
  - [7] S. Bohlens, B. Krüger, A. Drews, M. Bolte, G. Meier, and D. Pfannkuche, Current controlled random-access memory based on magnetic vortex handedness, *Appl. Phys. Lett.* **93**, 142508 (2008).
  - [8] V. Pribiag, I. Krivorotov, G. Fuchs, P. Braganca, O. Ozatay, J. Sankey, D. Ralph, and R. Buhrman, Magnetic vortex oscillator driven by dc spin-polarized current, *Nat. Phys.* **3**, 498 (2007).

- [9] H. Jung, Y.-S. Choi, K.-S. Lee, D.-S. Han, Y.-S. Yu, M.-Y. Im, P. Fischer, and S.-K. Kim, Logic operations based on magnetic-vortex-state networks, *Acs Nano* **6**, 3712 (2012).
- [10] K.-S. Lee, S. Choi, and S.-K. Kim, Radiation of spin waves from magnetic vortex cores by their dynamic motion and annihilation processes, *Appl. Phys. Lett.* **87**, 192502 (2005).
- [11] S. Wintz, V. Tiberkevich, M. Weigand, J. Raabe, J. Lindner, A. Erbe, A. Slavin, and J. Fassbender, Magnetic vortex cores as tunable spin-wave emitters, *Nat. Nanotechnol.* **11**, 948 (2016).
- [12] O. Tchernyshyov and G.-W. Chern, Fractional Vortices and Composite Domain Walls in Flat Nanomagnets, *Phys. Rev. Lett.* **95**, 197204 (2005).
- [13] B. Hillebrands and A. Thiaville, *Spin Dynamics in Confined Magnetic Structures ii* (Springer, Berlin, 2006), p. 161.
- [14] V. Estévez and L. Laurson, Magnetic domain-wall dynamics in wide permalloy strips, *Phys. Rev. B* **93**, 064403 (2016).
- [15] S. Gliga, Y. Liu, and R. Hertel, in *Journal of Physics: Conference Series*, Vol. 303 (IOP Publishing, 2011), p. 012005.
- [16] K. Y. Guslienko, K.-S. Lee, and S.-K. Kim, Dynamic Origin of Vortex Core Switching in Soft Magnetic Nanodots, *Phys. Rev. Lett.* **100**, 027203 (2008).
- [17] A. Vansteenkiste, K. Chou, M. Weigand, M. Curcic, V. Sackmann, H. Stoll, T. Tylliszczak, G. Woltersdorf, C. Back, and G. Schütz *et al.*, X-ray imaging of the dynamic magnetic vortex core deformation, *Nat. Phys.* **5**, 332 (2009).
- [18] B. Van Waeyenberge, A. Puzic, H. Stoll, K. Chou, T. Tylliszczak, R. Hertel, M. Fähnle, H. Brückl, K. Rott, and G. Reiss *et al.*, Magnetic vortex core reversal by excitation with short bursts of an alternating field, *Nature* **444**, 461 (2006).
- [19] R. Hertel, S. Gliga, M. Fähnle, and C. Schneider, Ultrafast Nanomagnetic Toggle Switching of Vortex Cores, *Phys. Rev. Lett.* **98**, 117201 (2007).
- [20] K.-S. Lee, S.-K. Kim, Y.-S. Yu, Y.-S. Choi, K. Y. Guslienko, H. Jung, and P. Fischer, Universal Criterion and Phase Diagram for Switching a Magnetic Vortex Core in Soft Magnetic Nanodots, *Phys. Rev. Lett.* **101**, 267206 (2008).
- [21] K. Yamada, S. Kasai, Y. Nakatani, K. Kobayashi, H. Kohno, A. Thiaville, and T. Ono, Electrical switching of the vortex core in a magnetic disk, *Nat. Mater.* **6**, 270 (2007).
- [22] M. Curcic, B. Van Waeyenberge, A. Vansteenkiste, M. Weigand, V. Sackmann, H. Stoll, M. Fähnle, T. Tylliszczak, G. Woltersdorf, and C. H. Back *et al.*, Polarization Selective Magnetic Vortex Dynamics and Core Reversal in Rotating Magnetic Fields, *Phys. Rev. Lett.* **101**, 197204 (2008).
- [23] M. Weigand, B. Van Waeyenberge, A. Vansteenkiste, M. Curcic, V. Sackmann, H. Stoll, T. Tylliszczak, K. Kaznatcheev, D. Bertwistle, and G. Woltersdorf *et al.*, Vortex Core Switching by Coherent Excitation with Single In-Plane Magnetic Field Pulses, *Phys. Rev. Lett.* **102**, 077201 (2009).
- [24] B. Pigeau, G. De Loubens, O. Klein, A. Riegler, F. Lochner, G. Schmidt, and L. W. Molenkamp, Optimal control of vortex-core polarity by resonant microwave pulses, *Nat. Phys.* **7**, 26 (2011).
- [25] K. Yamada, S. Kasai, Y. Nakatani, K. Kobayashi, and T. Ono, Current-induced switching of magnetic vortex core in ferromagnetic elliptical disks, *Appl. Phys. Lett.* **96**, 192508 (2010).
- [26] M. Kammerer, M. Weigand, M. Curcic, M. Noske, M. Sproll, A. Vansteenkiste, B. Van Waeyenberge, H. Stoll, G. Woltersdorf, and C. H. Back *et al.*, Magnetic vortex core reversal by excitation of spin waves, *Nat. Commun.* **2**, 279 (2011).
- [27] V. Estévez and L. Laurson, Fast vortex wall motion in wide permalloy strips from double switching of the vortex core, *Phys. Rev. B* **96**, 064420 (2017).
- [28] T. Sato, K. Yamada, and Y. Nakatani, Switching of magnetic vortex core in a pac-man disk using a single field pulse, *Appl. Phys. Express* **7**, 033003 (2014).
- [29] M.-W. Yoo, K.-S. Lee, D.-E. Jeong, and S.-K. Kim, Origin, criterion, and mechanism of vortex-core reversals in soft magnetic nanodisks under perpendicular bias fields, *Phys. Rev. B* **82**, 174437 (2010).
- [30] K.-S. Lee, M.-W. Yoo, Y.-S. Choi, and S.-K. Kim, Edge-Soliton-Mediated Vortex-Core Reversal Dynamics, *Phys. Rev. Lett.* **106**, 147201 (2011).
- [31] S.-K. Kim, Y.-S. Choi, K.-S. Lee, K. Y. Guslienko, and D.-E. Jeong, Electric-current-driven vortex-core reversal in soft magnetic nanodots, *Appl. Phys. Lett.* **91**, 082506 (2007).
- [32] A. Thiele, Steady-State Motion of Magnetic Domains, *Phys. Rev. Lett.* **30**, 230 (1973).
- [33] M. Mehrnia, J. Trimble, and J. Berezovsky, Three-dimensional frequency-and phase-multiplexed magneto-optical microscopy, *Opt. Express* **27**, 33942 (2019).
- [34] R. Badea and J. Berezovsky, Mapping the Landscape of Domain-Wall Pinning in Ferromagnetic Films Using Differential Magneto-Optical Microscopy, *Phys. Rev. Appl.* **5**, 064003 (2016).
- [35] D. Schreiber, O. Heinonen, and A. Petford-Long, Micro-magnetic modeling of the magnetization dynamics in a circularly exchange-biased and exchange-coupled ferromagnetic multilayer, *Phys. Rev. B* **80**, 014411 (2009).
- [36] R. Compton and P. Crowell, Dynamics of a Pinned Magnetic Vortex, *Phys. Rev. Lett.* **97**, 137202 (2006).
- [37] T.-Y. Chen, M. J. Erickson, P. Crowell, and C. Leighton, Surface Roughness Dominated Pinning Mechanism of Magnetic Vortices in Soft Ferromagnetic Films, *Phys. Rev. Lett.* **109**, 097202 (2012).
- [38] D. Bäuerle, in *Laser Processing and Chemistry*, (Springer, 2011), p. 581.
- [39] F. Hoffmann and H. Pascard, in *AIP Conference Proceedings*, (American Institute of Physics, 1972), Vol. 5, p. 1103.
- [40] M. Fitzsimmons, T. J. Silva, and T. Crawford, Surface oxidation of permalloy thin films, *Phys. Rev. B* **73**, 014420 (2006).
- [41] X. Dong, X. Song, S. Yin, M. M. Shirolkar, M. Li, and H. Wang, Probing the oxidation kinetics of small permalloy particles, *J. Solid State Chem.* **246**, 309 (2017).
- [42] See Supplemental Material at <http://link.aps.org/supplemental/10.1103/PhysRevApplied.16.034049> for movies of simulation results.
- [43] R. Silva, A. Pereira, R. Silva, W. Moura-Melo, N. Oliveira-Neto, S. Leonel, and P. Coura, Predicted defect-induced vortex core switching in thin magnetic nanodisks, *Phys. Rev. B* **78**, 054423 (2008).